New Journal of Physics
The open–access journal for physics

A model for noise effects on fibre tract trajectories in diffusion tensor imaging: theory and simulations

Marián Boguñá[1,2], Sinisa Pajevic[1], Peter J Basser[3] and George H Weiss[1,4]

[1] Mathematical and Statistical Computing Laboratory, DCB/CIT, National Institutes of Health, Bethesda, MD 20892, USA
[2] Departament de Física Fonamental, Universitat de Barcelona, Barcelona, Spain
[3] Section on Tissue Biophysics and Biomimetics, LIMB/NICHD, National Institutes of Health, Bethesda, MD 20892, USA
E-mail: ghw@helix.nih.gov

New Journal of Physics **7** (2005) 24
Received 17 August 2004
Published 31 January 2005
Online at http://www.njp.org/
doi:10.1088/1367-2630/7/1/024

Abstract. *In vivo* diffusion tensor data obtained with diffusion tensor magnetic resonance imaging (DT-MRI) can be used to estimate fibre tract trajectories in white matter in the brain. Such data can, for example, be used to visualize and study the connectivity and continuity of neural pathways in the central and peripheral nervous systems. This paper discusses a toy model which is used to assess limitations on the reliability of computed trajectories imposed by MRI noise. The analysis is based on a two-dimensional random walk model for which a very good approximate solution is available. The suggested theoretical approach to analyse this model is shown to be in excellent agreement with simulations.

Contents

[4] Author to whom any correspondence should be addressed.

PII: S1367-2630(05)85185-7

1. Background

Magnetic resonance imaging (MRI) is widely used in medicine and biology. One reason for this is the ability to combine MRI with other nuclear magnetic resonance (NMR) spectroscopic methods. One recent example is diffusion tensor MRI (DT-MRI) in which an NMR spectroscopic measurement of an effective diffusion tensor of water protons is performed in every voxel within an imaged volume [1, 2]. A unique characteristic of the diffusion tensor field as measured in DT-MRI is that it reflects structural and architectural features of the tissue.

These features of the diffusion tensor often change significantly due to disease processes so that DT-MRI has been used to characterize a large number of diseases, among which are ischaemia [3]–[6] multiple sclerosis [7], and Alzheimer's disease [8]. But more relevant for this work is that it is the first non-invasive imaging modality able to provide estimates of fibre-tract trajectories in soft fibrous tissues as exemplified by brain white matter [1], [9]–[13].

This ability stems from the fact that the white matter in brain consists of the axonal fibre bundles in which the diffusion of water tends to be highly anisotropic. Consequently, the diffusion process cannot be described adequately by a single diffusion constant but requires at least a second-rank diffusion tensor (i.e., a 3×3 symmetric matrix), $\mathbf{D}$, whose components can be estimated from MRI data.

Intrinsic quantitative parameters can be extracted from DT-MRI data that characterize distinct features describing the size, shape, orientation or pattern of root-mean-squared (rms) displacement profiles within the imaged volume. Directional information can be obtained from the eigenvectors of $\mathbf{D}$, which define the orientations of local principal axes. Colour maps that indicate the local fibre-tract orientation are created by combining information contained in the eigenvector associated with the largest eigenvalue, or principal diffusivity, together with a measure of diffusion anisotropy [14]–[16].

Fibre-tract trajectories can be constructed from tensor data by generating streamlines that follow the local direction of maximum apparent diffusivity [1], [9]–[13], [17]–[23]. While the details and implementations of these DT-MRI fibre tractography methods differ, they are all based on the same assumption that the eigenvector associated with the largest eigenvalue within a voxel points in the direction of the fibre tract [1]. The tract trajectory is then determined by following these local direction vectors from point to point [13, 19].

However, background noise in diffusion-weighted images from which the diffusion tensor is estimated, places inherent physical limits on the accuracy and reliability of any fibre tract-following technique. This appears in the form of fluctuations in the fibre-field direction, which can cause the computed tracts to meander off course. This artifact has been demonstrated in simulations of tract following [13, 24, 25]. To date, there is no theory that relates the extent to which such errors depend on measured variables in the MRI experiment, such as the S/N ratio of the diffusion-weighted images or the diameter of the fibre tract.

In this paper we develop a highly idealized model, describing the effect of NMR noise on tract trajectory-following routines. One simplification entails replacing a curved fibre tract (figure 1(a)) by a right cylinder of radius R as in figure 1(b). The tract-following should, in the ideal noise-free case, produce a trajectory that lies along the centre of the fibre. In our idealization that represents the fibre tract by a cylinder, this means that the trajectory, in the absence of noise, lies along the cylinder axis. The model ignores the curvature of the axis and it only provides a rough estimate of the effects of background noise.

2. Description of fibre tract trajectories

A fibre trajectory can be represented as a three-dimensional space curve, i.e., as a vector $\mathbf{r}(s)$ parametrized by the distance along the fibre, s. The equation relating $\mathbf{r}(s)$ to the unit tangent vector at s, $\mathbf{t}(s)$, is [26]

$$\frac{\mathrm{d}\mathbf{r}(s)}{\mathrm{d}s} = \mathbf{t}(s). \tag{1}$$

Let the diffusion tensor at a given value of s be denoted by $\mathbf{D}(s)$.

To make use of the relation in equation (1), one needs to specify a second relation between $\mathbf{r}(s)$ and $\mathbf{t}(s)$. For this purpose we adopt the hypothesis advanced in [2] that the normalized eigenvector $\boldsymbol{\varepsilon}_1$ corresponding to the largest eigenvalue of $\mathbf{D}(s)$ lies parallel to the local fibre-tract direction. Several groups have confirmed the hypothesis to within acceptable error for heart tissue [27, 28]. A mathematical form of the hypothesis is written as

$$\mathbf{t}(s) = \boldsymbol{\varepsilon}_1 [\mathbf{r}(s)], \tag{2}$$

which is substituted into equation (1) to yield a system of three equations for $\mathbf{r}(s)$ subject to an initial condition $\mathbf{r}(0) = \mathbf{r}_0$. In practice, the resulting equations cannot be solved in closed form, and therefore require a numerical solution [13, 19]. An additional difficulty in solving equation (1) is the fact that the diffusion tensor eigenvectors are antipodally symmetric, so that both $\boldsymbol{\varepsilon}_1$ and $-\boldsymbol{\varepsilon}_1$ are equally valid solutions. This problem is solved by tracking in two opposite directions from a given starting point and choosing the sign that preserves the direction of the eigenvector in the previous step.

3. Analysis of the idealized model

The computed direction vector for the trajectory at any point will equal the true vector, i.e., the vector in the absence of noise, plus a random vector. Since the noise-corrupted trajectory is the sum of the true vectors plus the sum of the random vectors, the computed trajectory will always deviate from the true trajectory. A natural question is then how long a trajectory can be followed before the deviation becomes significant. To answer this question we derive pertinent results for a first-passage time problem. A good introduction to this class of problems can be found elsewhere [29]. In the present instance, we define the first-passage problem as that of finding the number of steps needed for the random walk to reach the circumference of the idealized right-circular cylinder boundary. It is also possible to transform this result into the problem of finding the distribution of the time, rather than the step number at which the random walk reaches the circumference for the first time.

Figure 1 illustrates how the fibre-tracking problem can be cast as a random walk on a circle of radius R. First, the actual tracked fibres (figure 1(a)) are approximated by right-circular cylinders (figure 1(b)), or more correctly, by three-dimensional tubes. Note that this approximation works well if we assume that the radius of curvature of the given tube is much larger than the single tracking step size, L (see figure 1(b)) and thus fibre tracts are viewed as right-circular cylinders. The fibre tract will be said to be followed accurately over the range $(0, s_{\max})$ provided that the

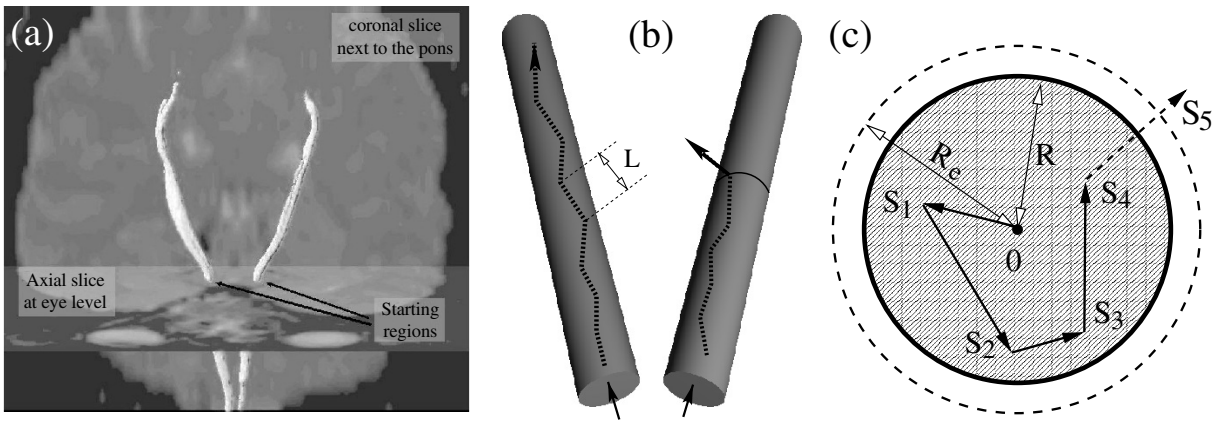

Figure 1. (a) A fibre tract obtained using the methodology in [13] which follows the principal direction of the tensor associated with the largest principal diffusivity. These tracts represent motor fibre pathways leading from the spinal cord, through the pons, up to the motor areas in the cortex of the brain. This tract is displayed against two MRI slices, one coronal (the plane parallel to ones face) and one axial (the plane perpendicular to body axis). (b) An idealized representation of the tracts as cylinders. Note that cylinders can curve in space; our assumption is that locally, at the level of a few tracking steps they appear as right-circular cylinders. (c) Assuming the locally cylindrical fibre shape, the fibre tracking of the noisy tensor field can be described as a random walk [30] on a disc with radius R. We later show that this can be approximated with a diffusion process with extrapolated absorbing boundary R_e.

measured tract vector never falls outside the cylinder of radius R in that range. If the cylinder is viewed head-on then the projection of each vector on the circle can be viewed as a single step of a random walk as shown in figure 1(c). This rephrases the analysis in terms of a first-passage time problem in which the time is replaced by the distance s.

Each step is a projection of a three-dimensional vector of fixed length, L, hence the length of each projected step is a random variable that takes on values between 0 and L. The result of simulating the noise properties of the three-dimensional eigenvectors (random walks) obtained from DT-MRI indicated that to a good approximation the distribution of the projected length is Gaussian and that of the turn angle is uniformly distributed over $(-\pi, \pi)$. Figure 2 shows results of simulations and their fits to the Gaussian distribution. It shows that for typical experimental settings it is safe to assume that the step lengths of the two-dimensional random walk are normally distributed. The standard deviations, σ, for different experimental settings are indicated in each graph of figure 2. Since the problem possesses cylindrical symmetry, we only show a one-dimensional slice, in the x direction, but the results were confirmed for an arbitrary direction, as well as the fact that the turn angle was uniformly distributed.

The problem of estimating the distribution of the number of steps in which the fibre tract can be followed accurately is therefore equivalent to that of finding the probability distribution of the number of steps required for a random walker in two dimensions, initially at the origin of the circle, to reach the circular boundary at radius R. We have found a very accurate approximation to the solution in terms of a similar problem for two-dimensional Brownian motion.

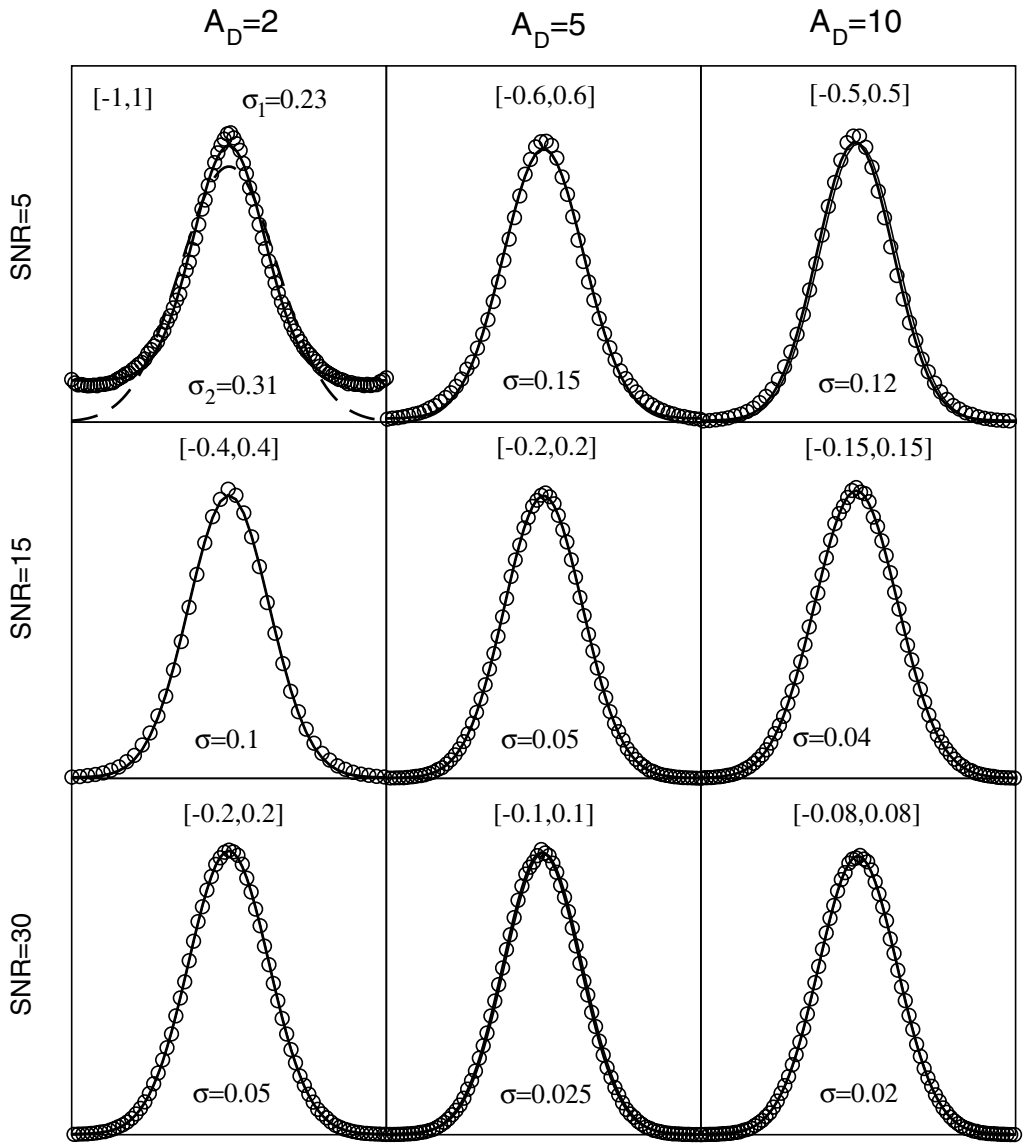

Figure 2. Simulated data (open circles) and best Gaussian fits to these data for nine probability densities for the x component of $\boldsymbol{\varepsilon}_1$, the eigenvector corresponding to the largest eigenvalue. The numbers in square brackets indicate the x-axis range. The noise-free $\boldsymbol{\varepsilon}_1$ points in the z direction. The components of $\boldsymbol{\varepsilon}_1$ have been normalized to 1 and their values can never fall outside the interval $[-1, 1]$. The simulations are for a tensor oriented along the z-axis and A_D is the anisotropy factor defined in terms of the three eigenvalues as $A_D = 2\lambda_1/(\lambda_2 + \lambda_3)$. The simulations were generated from a total of one million noisy tensors using typical experimental settings for DT-MRI. The distributions were fit to two types of Gaussian distributions with (σ_1) and without (σ_2 or σ) allowance for a nonzero baseline. Only in the case of small anisotropy and low SNR was this offset required to fit the data correctly. In typical fibre-tracking data, SNR is almost always higher than 15 and for the white matter fibres A_D is typically >2, usually in the range (2,10).

The type of random walk used in the present study is sometimes referred to as a Pearson random walk [30, 31], which plays an important role in crystallographic applications [32, 33]. To date, only properties of the probability density for the end-to-end distance of the random walker in an infinite plane have been analysed; there are no comparable results available for the corresponding first-passage time problem. Because of this stumbling block we have developed an approximation which we show to be in excellent agreement with simulated data, and depends on the dimensionless ratio $r_s = R/\sigma$.

In brief, we replace the full problem of the Pearson random walk by a standard two-dimensional diffusion problem with absorbing boundary condition. By adopting the diffusion approximation, we implicitly assume that the probability to find the walker at the boundary is zero. However, this is not the case in the original problem since there is always a finite probability that the walker arrives at the boundary in a single jump. This problem can be overcome by extrapolating the absorbing boundary beyond R and setting it to $R_e > R$ which requires that the solution to the diffusion equation vanishes at $r = R_e$ (see figure 1(c)). Results of our analysis are expressed in terms of the average length of the projection of a three-dimensional vector of fixed length (L) on the circle. We denote this average projected length as $\langle l \rangle$, which is related to the standard deviation, σ, of the random walk by $\langle l \rangle = (\pi/2)^{1/2}\sigma$. We expect the diffusion approximation to be useful when $\langle l \rangle \ll R_e$. Let ϑ be the relative difference between the extrapolated and the real radius:

$$\vartheta = \frac{R_e}{R} - 1. \tag{3}$$

We choose the value of R_e that best fits the solution to the simulated data. The probability that the projected vectors have not left the circle in m steps will be denoted by S_m which can be regarded as the probability that the tract has been successfully followed when m steps have been made. Our approximation consists of replacing a rather complicated iteration equation by an isotropic diffusion equation using an absorbing boundary condition at R_e. Initially the diffusing particle is found at $r = 0$. In this way, we find an approximation to this probability that closely reproduces the simulated data and can be expressed as the infinite series:

$$S_m = \frac{2}{1+\vartheta} \sum_{n=1}^{\infty} J_1\left(\frac{\alpha_n}{1+\vartheta}\right) \left[\alpha_n J_1^2(\alpha_n)\right]^{-1} \exp\left[-\frac{m}{\tau_c(n)}\right], \quad m \geqslant 1. \tag{4}$$

Here $J_1(u)$ is a Bessel function of order 1, α_n are the successive roots of $J_0(\alpha) = 0$, [34] and $\tau_c(n)$ is the characteristic length/time defined as $\tau_c(n) = \pi(R_e/\alpha_n\langle l \rangle)^2$.

Since the parameter m appears only in the exponential in equation (4) the series representation of S_m allows us to calculate moments of the number of steps required to leave the circle. For example, the average number of steps before passing through the circumference of the circle is

$$\langle m \rangle = \sum_{m=0}^{\infty} S_m = \frac{2}{1+\vartheta} \sum_{n=1}^{\infty} J_1\left(\frac{\alpha_n}{1+\vartheta}\right) \left[\alpha_n J_1^2(\alpha_n)\right]^{-1} \left[1 - \exp\left(-\frac{m}{\tau_c(n)}\right)\right]^{-1} \tag{5}$$

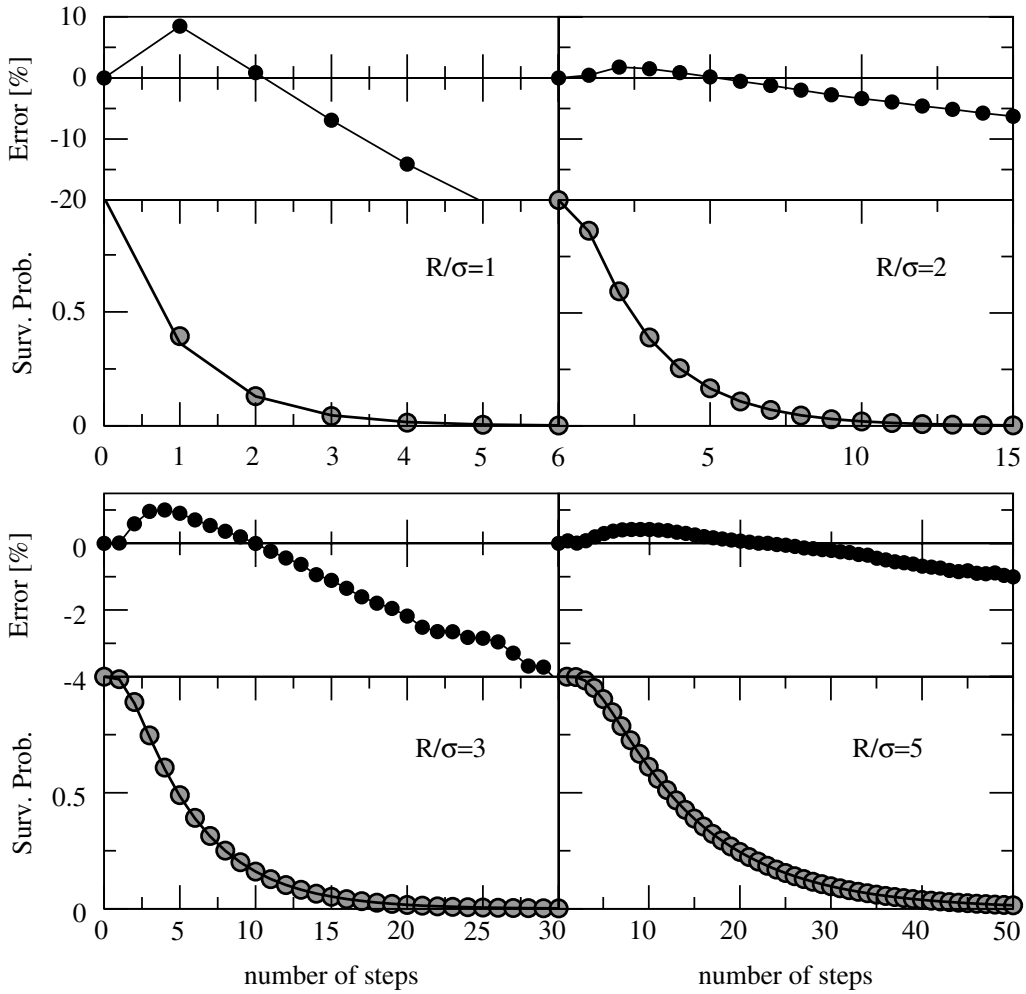

Figure 3. A comparison of the diffusion theory-based approximation for the survival probability (solid line) in equation (4) with Monte Carlo simulations (shaded circles) for four different values of r_s as indicated in the figures. The graphs above indicate the percentage difference between the simulations and the theoretical prediction. Only five terms of the series for S_m were used to generate the theoretical curve and 30 million random walkers were used to obtain the Monte Carlo estimate. The ϑ values used for small ratios, $r_s(<2)$, are obtained from a slightly more precise empirical formula $\vartheta = 0.67/r_s^{1.08}$.

and the corresponding second moment is

$$\langle m^2 \rangle = \sum_{m=0}^{\infty} (2m+1) S_m = \frac{2}{1+\vartheta} \sum_{n=1}^{\infty} J_1\left(\frac{\alpha_n}{1+\vartheta}\right) \left[\alpha_n J_1^2(\alpha_n)\right]^{-1} \times \left[1 + \exp\left(-\frac{m}{\tau_c(n)}\right)\right] \left[1 - \exp\left(-\frac{m}{\tau_c(n)}\right)\right]^{-2}. \quad (6)$$

A comparison of these expressions for S_m and the moments with results of simulations is given in figure 3. The results of the comparison could hardly be more satisfactory. Note that the plotted

errors are relative errors. The large percentage errors that occur for $r_s = 1$ are in the region in which $S_m \approx 0$ and therefore do not significantly influence the calculation of moments. The optimal value of R_e to be used depends on the ratio $r_s = R/\sigma$. We found empirically that ϑ in equation (3) is approximately equal to $\vartheta = 0.6/r_s$. If one is to use this formula in practice, the estimates for R and σ can be derived using a combination of experimental data together with data-based simulations. As an example, if one is to track a fibre with $R = 2$ mm using data acquired on a grid with $2 \times 2 \times 2$ mm (hence the fibre is only two voxels thick) and if we assume that its anisotropy is going to be $A_D = 5$ throughout the length of the fibre, then the expected tracking length would be ($\langle m \rangle \pm \sigma_m$): 5 ± 2 cm, 42 ± 30 cm, 164 ± 120 cm, respectively for SNRs of 5, 15, and 30. In practice, tracking will generally be less reliable than this, due to other sources of noise and the effects of the fibre tract curvature (biased departure from the desired trajectory) but these estimates can serve as upper bounds on how long one can expect to track a fibre.

4. Discussion

In this paper we have suggested an ideal model, based on the theory of first-passage times for random walks, to quantitate the errors in trajectory-following of fibre tracts by DT-MRI. One of the more interesting results emerging from our simulations is a suggestion that deviation from the true trajectory, or the random walk on a disc, is very well-described using the diffusion limit even for surprisingly small ratios of R and σ. One reason for this is that the maximum of the Gaussian distribution occurs at $r = 0$, which is roughly equivalent to the necessary condition for the central-limit theorem to hold. It is difficult to give a rigorous argument to justify this conclusion.

It must be borne in mind that we have idealized the fibre tract to be a straight line, and phrased the problem as being that of finding the statistical characteristics of the number of steps taken by a random deviation vector (i.e., the difference between the true trajectory and the estimated one) before it reaches a preset distance. The problem is therefore equivalent to one in the theory of first-passage times, which seeks distribution of the number of steps taken by a random walk consisting of random step lengths to escape from a circle. We conjecture that since actual fibres are curved, the first passage time/distance will be smaller than our estimates which we treat as upper bounds on how long one can expect to track a fibre successfully. However, when the radius of curvature of the given fibre is much larger than the single tracking step size L, this approximation works well.

The problem studied is also idealized in other respect, ignoring several known complexities and artifacts that may be present [11, 13]. It is known that background noise in DT-MRI data can cause the eigenvalues to be mis-classified when sorted by magnitude in each voxel [35]. This can cause a mis-classification of the corresponding eigenvectors [36]. While the mis-sorting of eigenvalues is relatively rare in coherent white matter tracts at a high SNR, it occurs more frequently in less coherently organized white matter regions. When this occurs, $\boldsymbol{\varepsilon}_1[\mathbf{r}(s)]$ no longer points along the true fibre direction, which, in turn, causes the computed trajectory to veer off course i.e., may cause a 90° deviation and a consequent jump to an adjacent tract. This type of error is not encompassed in our present analysis. To give a more complete analysis of all of the errors possible in DT-MRI would require a heavy investment in both experiment and simulations. Nevertheless, we believe that our present analysis is a first step in the process and provides order-of-magnitude estimates of expected errors in trajectory-following, at least in the high-SNR regime.

It is worthwhile noting the strong dependence of $\langle m \rangle$ on SNR over a range of values of this quantity widely used in MRI applications. This point has not been made by other groups.

References

[1] Basser P J *et al* 1994 MR diffusion tensor spectroscopy and imaging *Biophys. J.* **66** 259–67

[2] Basser P J *et al* 1994 Estimation of the effective self-diffusion tensor from the NMR spin echo *J. Magn. Reson.* B **103** 247–54

[3] Zelaya F *et al* 1999 An evaluation of the time dependence of the anisotropy of the water diffusion tensor in acute human ischemia *Magn. Reson. Imag.* **17** 331–48

[4] Jones D K *et al* 1999 Characterization of white matter damage in ischemic leukoaraiosis with diffusion tensor MRI *Stroke* **30** 393–7

[5] Mukherjee P *et al* 2000 Differences between gray matter and white matter water diffusion in stroke: diffusion-tensor MR imaging in 12 patients *Radiology* **215** 211–20

[6] Sotak C H 2002 The role of diffusion tensor imaging in the evaluation of ischemic brain injury—a review *NMR Biomed.* **15** 561–9

[7] Horsfield M A and Jones D K 2002 Applications of diffusion-weighted and diffusion tensor MRI to white matter diseases—a review *NMR Biomed.* **15** 570–7

[8] Rose S E *et al* 2000 Loss of connectivity in Alzheimer's disease: an evaluation of white matter tract integrity with colour coded MR diffusion tensor imaging *J. Neurol. Neurosurg. Psychiatry* **69** 528–30

[9] Conturo T E *et al* 1999 Tracking neuronal fiber pathways in the living human brain *Proc. Natl Acad. Sci. USA* **96** 10422–7

[10] Poupon C *et al* 1999 Tracking white matter fascicles with diffusion tensor imaging *Proc. 8th Annual Meeting of the ISMRM (Sydney)*

[11] Mori S *et al* 1999 Three-dimensional tracking of axonal projections in the brain by magnetic resonance imaging *Ann. Neurol.* **45** 265–9

[12] Mori S *et al* 2000 *In vivo* visualization of human neural pathways by magnetic resonance imaging *Ann. Neurol.* **47** 412–4

[13] Basser P J *et al* 2000 *In vivo* fiber-tractography in human brain using diffusion tensor MRI (DT-MRI) data *Magn. Reson. Med.* **44** 625–32

[14] Jones D K 1997 Full representation of white-matter fibre direction on one map via diffusion tensor analysis *ISMRM Proc.* **3** 1743

[15] Pierpaoli C 1997 Oh No! One more method for color mapping of fiber tract direction using diffusion MR imaging data *ISMRM Proc.* **3** 1741

[16] Pajevic S and Pierpaoli C 1999 Color schemes to represent the orientation of anisotropic tissues from diffusion tensor data: application to white matter fiber tract mapping in the human brain *Magn. Reson. Med.* **42** 526

[17] Wedeen V J *et al* 1995 White matter connectivity explored by MRI *Proc. 1st Int. Conf. for Functional Mapping of the Human Brain (Paris)*

[18] Wedeen V J 1996 Diffusion anisotropy and white matter tracts *Second Brain Map Meeting (Boston)*

[19] Basser P J 1998 Fiber-tractography via diffusion tensor MRI (DT-MRI) *Proc. 6th Annual Meeting of the ISMRM (Sydney, AU)*

[20] Poupon C *et al* 1998 Regularization of MR diffusion tensor maps for tracking brain white matter bundles *Proc. MICCAI'98*

[21] Jones D K *et al* 1998 Non-invasive assessment of structural connectivity in white matter by diffusion tensor MRI *Proc. 6th Annual Meeting of the ISMRM (Sydney)*

[22] Jones D K *et al* 1999 Non-invasive assessment of axonal fiber connectivity in the human brain via diffusion tensor MRI *Magn. Reson. Med.* **42** 37–41

[23] Poupon C *et al* 2001 Towards inference of human brain connectivity from MR diffusion tensor data *Med. Image Anal.* **5** 1–15

[24] Lazar M and Alexander A L 2003 An error analysis of white matter tractography methods: synthetic diffusion tensor field simulations *Neuroimage* **20** 1140–53
[25] Lazar M *et al* 2003 White matter tractography using diffusion tensor deflection *Hum. Brain Mapp.* **18** 306–21
[26] Kreyszig E 1968 *Introduction to Differential Geometry and Riemannian Geometry* (Toronto: University of Toronto Press; reprinted by Dover, New York, 1991)
[27] Hsu E *et al* 1998 Magnetic resonance myocardial fiber-orientation mapping with direct histological correlation *Am. J. Physiol.* **274** H1627–H1634
[28] Scollan D *et al* 1998 Histological validation of myocardial microstructure obtained from diffusion tensor magnetic resonance imaging *Am. J. Physiol.* **275** H2308–H2318
[29] Redner S 2001 *A Guide to First-Passage Processes* (Cambridge: Cambridge University Press)
[30] Pearson K 1905 The problem of the random walk *Nature* **72** 294
[31] Weiss G H 1994 *Aspects and Applications of the Random Walk* (Amsterdam: North-Holland)
[32] Giacovazzo C 1980 *Direct Methods in Crystallography* (London: Academic)
[33] Shmueli U and Weiss G H 1995 *Introduction to Crystallographic Statistics* (Oxford: Oxford University Press)
[34] Abramowitz M and Stegun I A 1970 *Handbook of Mathematical Functions* (New York: Dover)
[35] Pierpaoli C *et al* 1996 Diffusion tensor MR imaging of the human brain *Radiology* **201** 637–48
[36] Basser P J and Pajevic S 2000 Statistical artifacts in diffusion tensor MRI (DT-MRI) caused by background noise *Magn. Reson. Med.* **44** 41–50